Accurate and Computationally Efficient Aggregated Modelling of Offshore Wind Farms for Grid Compliance

Muhammad Helal Uddin, *Student Member, IEEE,* Junaid Khalid, *Student Member, IEEE,* Michael Smailes, *Member, IEEE,* Jun Liang, *Fellow, IEEE,* Sheng Wang, *Senior Member, IEEE*

***Abstract*—Detailed electromagnetic transient models of offshore wind farms incorporate the individual wind turbine dynamics and controls of many wind turbines (WTs), resulting in substantial computational burdens. This limits their practicality for large-scale system studies. While aggregation techniques reduce this burden, they often compromise accuracy, particularly in capturing dynamic behaviour during power system disturbances. To overcome this challenge, this paper proposes a gaussian mixture model clustering with information-theoretic averaging to group similar WTs and derive representative aggregated models. A structured eigenvalue sensitivity analysis is conducted to identify the control parameters that have the greatest impact on system dynamics, reducing the dimensionality of the parameter space. Additionally, an improved multi-objective gradient descent optimisation strategy is developed to identify and provide optimal values of system and control parameters under varying wind conditions and fault scenarios to ensure accuracy. The proposed modelling applicability is further demonstrated through assessment on an HVDC connected offshore wind farm under large disturbance and weak grid conditions in the time and frequency domains. Finally, the aggregated model's performance is validated against the detailed benchmark to ensure UK's grid compliance on modelling, confirming its ability to replicate key dynamic and steady-state characteristics with substantially reduced computational effort.**

***Index Terms*—Aggregation modelling, parameters sensitivity, multi-objective optimisation, grid compliance modelling.**

I. Introduction

As wind energy integration continues to rise globally, ensuring the dynamic performance and control of large-scale wind farms (WFs) has become crucial for the secure and stable operation of modern power systems. In power system studies, a detailed model of a WF typically includes the control systems of every wind turbine (WT), power converter switching operations, and electrical cable interconnections. While such detailed models are highly accurate, they significantly increase the computational burden in electromagnetic transient (EMT) simulations. Consequently, employing detailed models in large-scale system studies is often impractical and computationally intensive. Instead, a large number of WTs could be modelled by aggregation [1]. This study employs Type-4 full converter based permanent magnet synchronous generator (PMSG) wind turbines, which dominate modern offshore installations due to their high reliability in direct drive configurations and their superior controllability for meeting stringent grid compliance standards.

To provide a clearer synthesis of prior work and its limitations, existing wind farm aggregation methods can be organised into three methodological categories: reduced-order modelling, clustering-based aggregation, and learning-based or surrogate approaches. Within reduced-order modelling approaches, these range from single-machine equivalents, which model the WF as one scaled WT, to more accurate but computationally intensive multi-machine models, where turbines are grouped based on shared operational characteristics [1]. Although these methods simplify WF representation, the complexity in modelling and aggregation of wind farms (WFs) due to the stochastic nature of the wind, variability of wind speed and interactions between wind turbines is further complicated by different WF layouts and potential changes in the operating mode of WTs (i.e., normal, LVRT, disconnected) during faults in transmission lines [2].

For clustering-based aggregation methods, researchers have explored capacity-weighted techniques, probabilistic clustering, aggregated impedance models, and admittance model-order reduction. However, these approaches still suffer from reduced accuracy, limited generality, and restricted applicability [3]–[5]; especially for impedance based methods that are valid only for high-frequency oscillation analysis and do not capture EMT-level dynamic behaviour [6]. Moreover, traditional clustering methods based on single time snapshots often fail to capture time-evolving turbine dynamics, leading to reduced model fidelity over extended simulation periods. Several studies on clustering-based aggregation modelling have been conducted to address this such as fuzzy clustering–based multi-machine dynamic equivalent to analyse the active power characteristics of DFIG based wind farms in [5] and a geometric template matching based aggregation method which improves accuracy but increases computational overhead, slower convergence rate [7].

However, even with optimal clustering, accurate dynamic aggregation also depends on appropriate parameter identification. This is particularly challenging when dealing with a high number of interrelated control and physical parameters. Phasor Measurement Unit (PMU) based parameter identification methods are widely used to optimise wind turbine generator (WTG) parameters by minimising the mismatch in active and reactive power at the point of common coupling (PCC) between detailed and Phasor aggregated wind farm models [3],

M.H. Uddin, J. Khalid, and J. Liang (corresponding author, email: LiangJ1@cardiff.ac.uk) are with the School of Engineering, Cardiff University, CF24 3AA Cardiff, U.K.
M. Smailes is with Offshore Renewable Energy Catapult, NE24 1LZ Blyth, Northumberland, U.K.
S.Wang (corresponding author, email: Sheng.Wang@glasgow.ac.uk) is with the James Watt School of Engineering, University of Glasgow, G12 8QQ Glasgow, U.K.
This work was supported by the Engineering and Physical Sciences Research Council [grant number EP/X031144/1]. Project title: Accelerating the deployment of offshore wind using DC technology (ADOreD).

[8]–[10]. Existing approaches such as genetic algorithms [7], particle swarm optimisation (PSO) [11], and hybrid techniques [3], [8], [9] have been widely used, but often suffer from high computational cost and limited convergence efficiency. As a result, only a small set of dominant parameters are usually optimised, while the rest are either estimated empirically or fixed at nominal values [12], potentially degrading model accuracy under varying dynamic conditions.

More recently, physics informed learning approaches have been introduced for wind farm aggregation. These include PINN-based dynamic identification and symbolic-regression/PDE-FIND frameworks that refine generic aggregated models using physical error mechanisms, thereby improving transient accuracy while keeping the model interpretable [13]. However, these symbolic-regression based physical-informed methods still depend heavily on high-quality operation data and predefined structural constraints, and their accuracy can degrade when capturing multi-timescale EMT dynamics or large parameter disparities across turbines [14]. Emerging Koopman operator and neural network assisted approaches have also been explored, where PINNs serve as nonlinear function approximators to provide observables for koopman lifting. However, these methods require carefully defined initial and boundary conditions to avoid local convergence issues, do not yield analytical equations, and often lead to high model complexity [15], [16]. Thus, while Koopman-based reduction is a promising direction, its application to large scale EMT level wind farm aggregation remains limited and underscores the need for approaches that balance interpretability and physical completeness.

Purely data-driven surrogate models also struggle with physical interpretability, especially when conducting small-signal analysis using eigenvalue or frequency-domain techniques [17], [18]. In contrast, eigenvalue sensitivity offers a computationally efficient approach for assessing the impact of parameter variations on system stability, as it relies on linear algebra applied to linearised system matrices at equilibrium points, rather than computationally intensive time-domain simulations for each parameter perturbation in trajectory sensitivity method [5], [7]. This sensitivity analysis is crucial for identifying the key parameters that significantly influence dynamic response, thereby allowing optimisation efforts to be focused and avoiding the waste of computational resources on less impactful parameters. For the subsequent fine tuning of these identified parameters, Multi-Objective Gradient Descent (MOGD) is well-suited to this application due to the characteristics of the formulated identification problem and the need for high computational efficiency. Fast convergence and low memory demand for smooth and convex optimisation problems make it effective for wind farm aggregation parameter tuning.

This becomes especially relevant in light of the UK grid operator's requirements introduced after the major blackout on August 2019, which highlighted the need for more accurate dynamic modelling. As a result, all generation projects completed after September 2022 must submit EMT models to the Electricity System Operator (ESO) [19]. Furthermore, wind farms must comply with stringent dynamic performance criteria outlined in GCO141 of the UK grid code, including voltage regulation, fault ride-through, and frequency response during and after grid disturbances [19]. While aggregation accuracy and grid code compliance have been studied separately [20], to the best of my knowledge the only work linking aggregation errors to transient stability under compliance tests is based on China's grid code [21]. This highlights a clear research gap in assessing how aggregation errors may affect grid compliance of ENTSO-E, the UK grid code and industry approved standards.

Therefore, there remains a pressing need for an aggregation framework that can accurately reproduce EMT level dynamics while remaining computationally efficient and fully compatible with grid code compliance studies. Existing reduced-order, clustering-based, and learning-based methods either oversimplify key converter and control dynamics, fail to generalise across varying wind and fault conditions, or lack the interpretability required for stability assessment and compliance verification. Moreover, no existing approach provides a systematic link between aggregation errors, parameter sensitivities, and the dynamic performance criteria mandated by the UK grid code. This gap motivates the present study, which aims to develop an aggregation methodology that enhances modelling fidelity, improves parameter identification, and ensures robust compliance with grid code requirements. The main contributions of this paper are:

1) A PMSG-based WF is first reduced to a smaller set of aggregated equivalents using Gaussian Mixture Model (GMM) clustering with Information-Theoretic Averaging (ITA) to enhance modelling accuracy while ensuring computational efficiency.
2) Based on this reduced-order representation, a systematic eigenvalue sensitivity analysis is applied to identify key control parameters which are most critical to dynamic behaviour, reducing parameter dimensionality in the aggregation context.
3) These parameters are then tuned using a multi-objective gradient descent algorithm that integrates physics-guided modifications with an adaptive learning strategy to provide robust parameter identification under both wind and fault disturbances.
4) Finally, the model is validated against GCO141 UK grid code modelling requirements, to demonstrate its capability for industry compliant dynamic modelling.

The structure of this paper is organised as follows. Section II presents the GMM–ITA clustering framework used to generate representative wind turbine groups. Section III develops the aggregated wind farm model and introduces the eigenvalue based sensitivity analysis for selecting key control parameters. Section IV formulates and solves the multi-objective parameter identification problem using an improved gradient-descent approach. Section V evaluates the proposed aggregated model through dynamic simulations, applicability test with HVDC system and UK grid code compliance tests.

II. GMM–ITA based Aggregated Wind Farm Model

The complexity and accuracy of an aggregated model are strongly influenced by how the aggregation algorithm is defined and which indicators and parameters are selected for

inclusion in the final model. Clustering WTs is a proven strategy for improving the accuracy of WF aggregated models by reducing intra-cluster variability while preserving essential system dynamics [5]. This work adopts a GMM that offers flexible, scalable, and probabilistic clustering, capturing complex patterns more effectively and offering a more accurate representation of wind turbine behavior while being more computationally efficient for large datasets as it avoids the costly dendrogram construction required by traditional hierarchical approaches.

A. Clustering Indicator

Clustering indicators are specific time-series parameters, such as wind speed, active power, and terminal residual voltage of WT; used to group similar dynamic turbine behaviors across various operating conditions.

1) Wind Speed: Input wind speed critically determines wind turbine WT performance, correlating with geographical placement and wake effects. Hence, its time-series data is a primary clustering indicator. Fig. 1 presents the wind speed inputs of five representative turbines belonging to different clusters. These curves demonstrate how the wind varies across the wind farm because of wake effects and local turbulence. As upstream turbines extract kinetic energy from the wind, downstream units experience reduced and more variable wind speeds due to wake-induced effects, which are inherently reflected in the measured wind speed signals. By using these time-series signals, the clustering algorithm implicitly captures wake-induced correlations without the computational overhead of coupling explicit wake models directly into the EMT simulation environment.

2) Active Power: The operating characteristics of WTs vary continuously over time. To reliably represent their dynamic behavior, clustering indicators should capture the fluctuations in WT parameters. Among potential indicators, active power is widely regarded as the most representative of WT output performance [5]. Hence, the active power output is employed as a principal clustering criterion.

3) Terminal residual voltage: A well-designed equivalent collector network is essential for the aggregated model, as the dynamic response of each WT is influenced by line parameters and terminal residual voltages. Terminal residual voltages, measured on the low-voltage side of the step-up transformer as depicted in Fig. 2, are chosen as a clustering indicator because they reflect how line parameters and fault conditions in the collector network can cause errors in equivalent line impedance calculations ($Z_m = [Z_{W_{T_1}}, Z_{W_{T_2}}, ..., Z_{W_{T_m}}]$) due to the parallel connection of the WTs.

Other variables were excluded due to strong correlations with these indicators. Specifically, reactive power is tightly coupled to terminal voltage, converter currents are embedded in active power dynamics, and pitch angle is only active above the rated wind speed and provides no discriminative value under sub-rated and disturbance conditions.

For the aggregated model, each cluster is excited by an equivalent wind speed input defined as the power-weighted mean of the individual turbine wind speeds as follows:

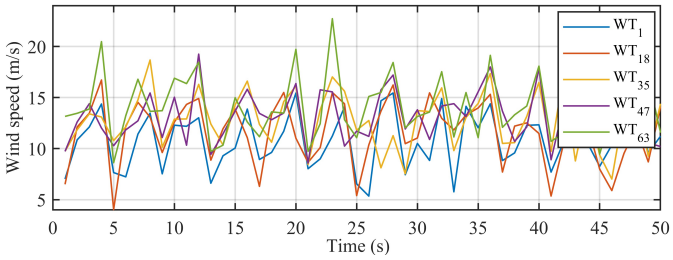

Fig. 1. Wind Speed curves of different WT.

$$v_{\text{eq}}^{(c)}(t) = \frac{\sum_{i \in W_c} P_i(t)\, v_i(t)}{\sum_{i \in W_c} P_i(t)} \tag{1}$$

where, $v_i(t)$ and $P_i(t)$ are the instantaneous wind speed and aerodynamic active power of turbine i in cluster W_c. In this way, turbines that produce more aerodynamic power (usually those with higher wind speeds) have a stronger influence on the representative wind speed, while turbines affected by wakes contribute less. This allows the aggregated model to capture partial turbine tripping implicitly, whereby turbines affected by faults contribute negligibly to the aggregated response, allowing the model to reflect reduced effective capacity at the wind farm level.

B. Clustering Algorithm

The proposed clustering framework is based on the well established GMM. The novelty lies in how this is applied to wind farm aggregation. (i) the use of time-series turbine indicators rather than static data (ii) the integration of ITA approach for more accurate cluster number selection.

The core steps of the GMM based algorithm are outlined below [22]:

Step 1: Each WT is represented by a feature vector based on three indicators: wind speed (x), active power (y), and residual terminal voltage (z).

$$\mathcal{X} = \{X_i\}_{i=1}^{n}, \qquad X_i = (x_i, y_i, z_i) \in \mathbb{R}^3,$$

Step 2: The GMM is initialised with k components (clusters) using k- means clustering which improves convergence of the subsequent expectation-maximization (EM) procedure. Each component is defined by a mean vector $\mu_k = [\mu_{x_k}, \mu_{y_k}, \mu_{z_k}]$, a covariance matrix Σ_k as well as mixing coefficient π_k indicating the weight of cluster k.

Step 3: Expectation-Maximization (EM) algorithm: This iterative procedure fits the GMM to the dataset by maximising the likelihood of the data. The EM algorithm is employed because it effectively handles the nonlinear, correlated, overlapping wind turbine behaviors through a probabilistic soft clustering framework. Unlike stochastic alternatives, EM provides a computationally efficient and parallelizable approach that ensures stable convergence for high dimensional time-series signals while maintaining lower model complexity [23]. It alternates between:

a) **Expectation step (E-step)**:

$$\gamma_{ik} = \frac{\pi_k \mathcal{N}\left(X_i \mid \mu_k, \Sigma_k\right)}{\sum_{j=1}^{K} \pi_j \mathcal{N}\left(X_i \mid \mu_j, \Sigma_j\right)} \tag{2}$$

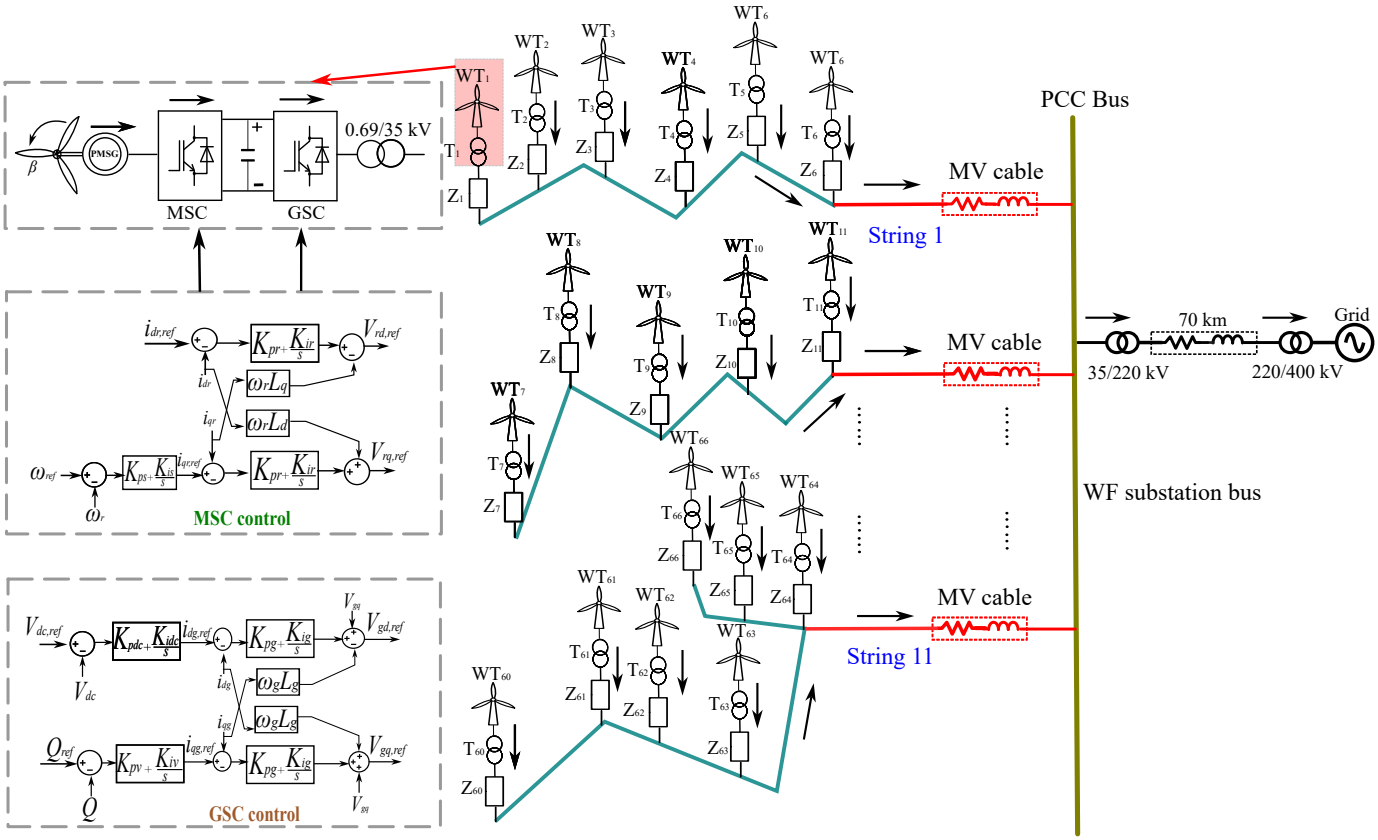

Fig. 2. Physical layout of WF with electrical connections considered in this study and control systems diagram.

where γi_k is the responsibility cluster k takes for data point i, and $\mathcal{N}(X_i \mid \mu_k, \Sigma_k)$ is the multivariate Gaussian probability density function.

b) **Maximization step (M-step)** : The EM algorithm updates each component's parameters (means μ_k, covariances Σ_k, and mixing weights π_k) using the responsibility values computed during the expectation step.

$$\begin{aligned} \mu_k &= \frac{1}{N_k}\sum_{i=1}^{n}\gamma_{ik}X_i \\ \Sigma_k &= \frac{1}{N_k}\sum_{i=1}^{n}\gamma_{ik}\left(X_i-\mu_k\right)\left(X_i-\mu_k\right)^T \\ \pi_k &= \frac{N_k}{n} \end{aligned} \tag{3}$$

Step 4: Repeat *Step 3* until convergence is achieved.

Step 5: After the EM algorithm converges, calculate the log-likelihood (LLL) of the model, which quantifies how well the GMM fits the data denoted by L.

$$\ln(L) = \sum_{i=1}^{n}\ln\left(\sum_{k=1}^{K}\pi_k\mathcal{N}\left(X_i \mid \mu_k, \Sigma_k\right)\right) \tag{4}$$

Step 6: The number of clusters k significantly influences aggregation fidelity and computational cost. To avoid overfitting (too many clusters) or underfitting (too few), the Akaike Information Criterion (AIC) and the Bayesian Information Criterion (BIC) are commonly applied methods [22].

$$\begin{aligned} \mathrm{AIC} &= 2\mathrm{p} - 2\ln(\mathrm{L}) \\ \mathrm{BIC} &= \mathrm{p}\ln(\mathrm{n}) - 2\ln(\mathrm{L}) \end{aligned} \tag{5}$$

Here, p denotes the number of parameters, which depends on the mixing weights, means, and covariance values, while n represents the total number of samples in the dataset.

When applied to the aggregated model for WTs, selecting a model with lower AIC would typically result in a more accurate model, but this could come at the cost of more clusters and potentially higher computational demand. On the other hand, a lower BIC suggests a model with fewer clusters (computationally faster) but penalises a more complex model (less accuracy).

For each $k = 1, \ldots, K_{\max}$, the EM algorithm was applied, AIC and BIC were computed, and the optimal k_{opt} was selected by minimising the chosen criterion. Since AIC tends to overestimate and BIC tends to underestimate the number of clusters, Information-Theoretic Averaging (ITA) is used to combine their strength [24]. It is based on the principle that instead of relying on a single model, we can average over a set of candidate models to account for uncertainty in model selection, leading to more robust estimates. This ensemble approach improves clustering stability, leading to more robust WT aggregation.

Each model is compared to the best one via:

$$\Delta_K = IC_K - \min_{K'} IC_{K'} \tag{6}$$

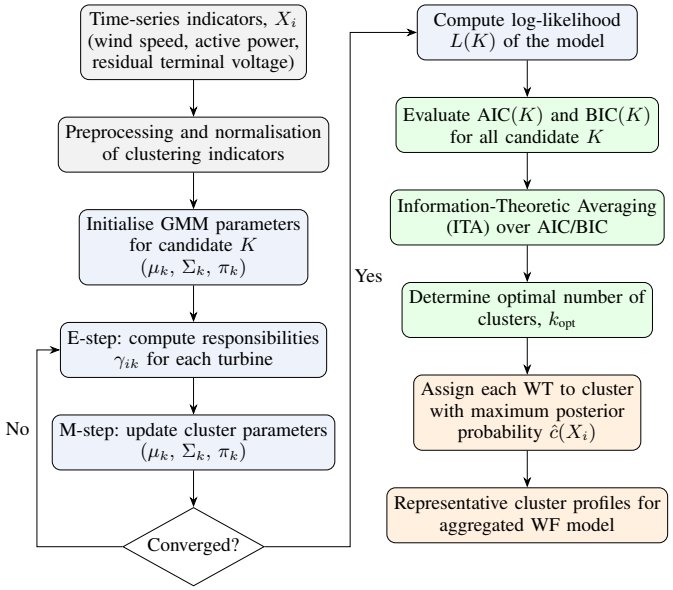

Fig. 3. The workflow of GMM–ITA clustering.

where, IC stands for information criterion (AIC or BIC), depending on which criterion is used. and assigned a weight:

$$w_K = \frac{\exp\left(-0.5 \cdot \Delta_K\right)}{\sum_{K'} \exp\left(-0.5 \cdot \Delta_{K'}\right)} \tag{7}$$

This provides a probabilistic weighting across models instead of relying on a single winner. Now, Responsibilities are averaged using ITA weights.

$$\bar{\gamma}_{ik} = \sum_K w_K \, \gamma_{ik}^{(K)} \tag{8}$$

Step 7 : Once the optimal cluster count k_{opt} is determined, each turbine is allocated to the cluster for which it shows the greatest responsibility, namely posterior probability.

$$\hat{c}(X_i) = \arg\max_k \, \bar{\gamma}_{ik} \tag{9}$$

Fig. 3 outlines GMM-ITA workflow for wind farm aggregation. Time series indicators derived from wind speed, active power, and terminal voltage are first preprocessed and used to train a GMM Model via EM algorithm. Information-theoretic criteria are then applied to determine an appropriate number of clusters, after which turbines are assigned based on maximum posterior probability and representative cluster profiles are extracted. This process enables the construction of an aggregated wind farm model that preserves essential dynamic characteristics under varying wind and fault conditions.

III. WF Aggregation Model Parameter Identification

A. Prioritising Key Parameters for Modelling

This paper addresses the challenge of handling a large number of control and generator parameters in aggregated models, which can hinder optimisation and reduce model interpretability. To overcome this, a systematic eigenvalue sensitivity analysis is performed. This targeted selection improves model accuracy identifying the most impactful parameters and enhances computational efficiency by reducing dimensionality.

B. Eigenvalue Sensitivity Analysis and Aggregated State-Space Modelling

After clustering the wind turbines using the GMM-ITA framework in section I, each wind turbine cluster is represented by a single reduced PMSG-based equivalent. The detailed dynamics of this equivalent, including drivetrain, pitch, converter, and DC-link subsystems, give rise to a differential algebraic model whose derivation is provided in Appendix B. By stacking the per cluster state vectors and incorporating the admittance matrix of the collector network at the PCC, the aggregated wind farm is expressed in the general form as follow:

$$\dot{X} = A_{\text{agg}} X + B_{\text{agg}} U \tag{10}$$

where, A_{agg} and B_{agg} are obtained after eliminating the algebraic voltage constraints (Appendix C). This aggregated state-space model provides a compact yet dynamically accurate representation of the wind farm and serves as the foundation for the eigenvalue based sensitivity analysis.

The dynamic behaviour of the reduced-order wind farm can be represented using differential algebraic equations (DAEs), which include state variables (X), input variables (U), and system parameters (ϕ) [25]. To evaluate how individual control parameters influence the small-signal behaviour of the aggregated wind farm, the model is linearised around its steady-state operating point (X_0,U_0). The resulting Jacobian matrix A_{agg} yields the characteristic equation

$$\det(\lambda \mathbb{I} - A_{\text{agg}}) = 0 \tag{11}$$

Here, $\mathbb{I}$ is the identity matrix. Solving (10) yields the system eigenvalues $\lambda_1, \lambda_2, \ldots, \lambda_n$ [26]. Because the elements of A_{agg} depend on the system parameters ϕ_j, the eigenvalues may be written as functions $\lambda_i(\phi_j)$. Variations in these parameters directly affect the associated eigenvalues and thus the dynamic performance of the aggregated model.

The sensitivity of eigenvalues to parameter ϕ_j is quantified as

$$\frac{\partial \lambda_i(\phi)}{\partial \phi_j} = q_i^{\mathrm{T}} \frac{\partial A_{\text{agg}}(\phi)}{\partial \phi_j} \, p_i \tag{12}$$

where q_i and p_i are the left and right eigenvectors corresponding to λ_i.

The state vector, X and input vector, U of the aggregated system are defined as:

$$\mathrm{X} = \begin{bmatrix} \omega_r, \beta, i_{dr}, i_{qr}, i_{dg}, i_{qg}, V_{dc}, i_{\text{int},dr}, i_{\text{int},qr}, i_{\text{int},dg}, i_{\text{int},qg}, \\ i_{\text{int},Vdc}, i_{\text{int},\omega_r}, i_{\text{int},\theta} \end{bmatrix}^T \tag{13}$$

$$\mathrm{U} = [i_{dr,ref} \; i_{qr,ref} \quad i_{dg,ref} \; i_{qg,ref} \; V_{dc,ref} \; \beta_{ref} \; \omega_{r,ref}]^T \tag{14}$$

$$\phi = [K_{pr} \; K_{ir} \; K_{pg} \; K_{ig} \; K_{ps} \; K_{is} \; K_{pp} \; K_{ip} \; K_{pdc} \; K_{idc} \; K_{pPLL} \; K_{iPLL} \; K_{pv} \; K_{iv}] \tag{15}$$

This formulation directly connects the clustering framework in Section II with the state-space representation in (13)–(15),

enabling a structured and computationally efficient application of eigenvalue sensitivity analysis. All nomenclature is given in Appendix A. Full derivations of the per-cluster model and aggregated matrices A_{agg} and B_{agg} are provided in Appendices B & C.

IV. Robust Key Parameter Identification Using Multi-Objective Methods

Following eigenvalue-based sensitivity analysis to identify most influential parameters, their values are accurately estimated using an improved MOGD optimisation algorithm.

A. Proposed Improved MOGD Algorithm for Key Parameters Optimisation

1) Problem formulation: We aim to identify the parameter vector $\boldsymbol{\theta} \in \mathbb{R}^n$ that minimises multiple objective functions:

$$\min_{\boldsymbol{\theta}} \mathbf{F}(\boldsymbol{\theta}) = \begin{bmatrix} F_1(\boldsymbol{\theta}) \\ F_2(\boldsymbol{\theta}) \\ F_3(\boldsymbol{\theta}) \\ F_4(\boldsymbol{\theta}) \end{bmatrix} \tag{16}$$

Subject to box constraints:

$$\theta_k^L \leq \theta_k \leq \theta_k^U, \quad \text{for } k = 1, 2, \ldots, n \tag{17}$$

- $F_1(\boldsymbol{\theta})$: Mean Squared Error (MSE) of active power during wind disturbance.
- $F_2(\boldsymbol{\theta})$: MSE of reactive power during wind disturbance.
- $F_3(\boldsymbol{\theta})$: MSE of active power during fault conditions.
- $F_4(\boldsymbol{\theta})$: MSE of reactive power during fault conditions.

2) Parameter vector and constraints: The parameter vector $\boldsymbol{\theta} \in \mathbb{R}^{14}$ comprises:

$$\boldsymbol{\theta} = \begin{bmatrix} P_{\text{rated}}, H, K_{\text{pr}}, K_{i\text{r}}, K_{\text{pg}}, K_{i\text{g}}, \\ K_{\text{ps}}, K_{i\text{s}}, K_{\text{pp}}, K_{i\text{p}}, K_{p\text{dc}}, K_{i\text{dc}} \end{bmatrix}^T \tag{18}$$

Each parameter θ_k has specified bounds $[\theta_k^L, \theta_k^U]$.

3) Weighted mean squared error: Each objective function $F_i(\boldsymbol{\theta})$ is computed as a weighted MSE to emphasise transient regions:

$$\text{MSE}_{P,\text{weighted}} = \frac{\sum_{t=1}^{T} W_p(t) \cdot (P_{\text{sim}}(t) - P_{\text{ref}}(t))^2}{\sum_{t=1}^{T} W_p(t)} \tag{19}$$

$$\text{MSE}_{Q,\text{weighted}} = \frac{\sum_{t=1}^{T} W_q(t) \cdot (Q_{\text{sim}}(t) - Q_{\text{ref}}(t))^2}{\sum_{t=1}^{T} W_q(t)} \tag{20}$$

Where, $W_p(t)$ and $W_q(t)$ are time-dependent weights assigning higher importance to transient regions.

4) Simulate enhanced model: The enhanced model adopts a physics-guided, data-driven hybrid approach. Instead of relying solely on statistical transformations, the method embeds known physical relationships and applies rate-based modifications to improve model fidelity, preserving transient dynamics of aggregated model.

- wind dip:

$$\frac{dP}{dt} = \frac{dP_{\text{ref}}}{dt} \cdot \frac{1.5}{H} \cdot \left(1 + 0.2 \cdot \left(1 - \frac{K_{p,\text{pitch}}}{35.6} \cdot \frac{K_{i,\text{pitch}}}{0.007}\right)\right) \tag{21}$$

- fault:

$$\frac{dP_{\text{fault}}}{dt} = \frac{dP_{\text{ref,fault}}}{dt} \cdot \frac{K_{p,\text{grid}}}{7.73} \cdot \frac{K_{i,\text{grid}}}{0.19} \cdot \frac{1.5}{H} \tag{22}$$

These coefficients (e.g., 7.73, 0.19 and 35.6) are normalisation factors obtained from the per-cluster reduced wind turbine EMT model via step response analysis and least squares fitting of the active power control channel. The resulting constants ensure that the aggregated model accurately matches the dynamic behavior of the detailed model, rather than being chosen empirically.

5) Gradient calculation: The gradient of each objective function with respect to parameters is approximated using central finite differences:

$$\frac{\partial F_i}{\partial \theta_j} \approx \frac{F_i(\boldsymbol{\theta} + h_j \mathbf{e}_j) - F_i(\boldsymbol{\theta} - h_j \mathbf{e}_j)}{2h_j} \tag{23}$$

Where:

- $\mathbf{e}_j$: Unit vector in the j-th direction.
- $h_j = 0.001 \cdot (\theta_j^U - \theta_j^L)$: Adaptive step size.

The gradients are organized into a matrix $\nabla \mathbf{F}(\boldsymbol{\theta}) \in \mathbb{R}^{n \times 4}$, where each column represents the gradient of one objective function:

$$\nabla \mathbf{F}(\boldsymbol{\theta}) = \begin{bmatrix} \frac{\partial F_1}{\partial \theta_1} & \frac{\partial F_2}{\partial \theta_1} & \frac{\partial F_3}{\partial \theta_1} & \frac{\partial F_4}{\partial \theta_1} \\ \frac{\partial F_1}{\partial \theta_2} & \frac{\partial F_2}{\partial \theta_2} & \frac{\partial F_3}{\partial \theta_2} & \frac{\partial F_4}{\partial \theta_2} \\ \vdots & \vdots & \vdots & \vdots \\ \frac{\partial F_1}{\partial \theta_n} & \frac{\partial F_2}{\partial \theta_n} & \frac{\partial F_3}{\partial \theta_n} & \frac{\partial F_4}{\partial \theta_n} \end{bmatrix} \tag{24}$$

6) Improved direction computation: The algorithm computes an improved descent direction that balances all objectives while considering parameter sensitivity and constraints. First, the weighted gradients are computed:

$$\nabla F_w(\boldsymbol{\theta}) = \sum_{i=1}^{4} w_i \nabla F_i(\boldsymbol{\theta}) \tag{25}$$

This is further refined by calculating parameter-specific weights based on:

- Parameter sensitivity: $S_j = \|\nabla F_j(\boldsymbol{\theta})\|$ where $\nabla F_j(\boldsymbol{\theta})$ is the j-th row of $\nabla \mathbf{F}(\boldsymbol{\theta})$
- Boundary awareness: boundary awareness B_j based on normalized position γ_j:

$$\gamma_j = \frac{\theta_j - \theta_j^L}{\theta_j^U - \theta_j^L} \tag{26}$$

$$B_j = \begin{cases} 1.0 + 2.0 \cdot (0.2 - \gamma_j), & \text{if } \gamma_j < 0.2 \\ 1.0 + 2.0 \cdot (\gamma_j - 0.8), & \text{if } \gamma_j > 0.8 \\ 1.0, & \text{otherwise} \end{cases} \tag{27}$$

- Combined weight: $\omega_j = B_j \cdot S_j$, with adjustments for critical parameters.

The directional derivatives for each objective are calculated as: $D_i = \nabla F_i(\boldsymbol{\theta})^T \cdot \nabla F_w(\boldsymbol{\theta})$

If $D_i < 0$ for any objective i (indicating a conflict), a modified direction is computed:

$$d_{\text{mod}} = \nabla F_w - \sum_{i: D_i < 0} \lambda_i D_i \cdot \frac{\nabla F_i}{\|\nabla F_i\|^2 + \epsilon} \tag{28}$$

TABLE I
COMPARISON OF THE PROPOSED MODEL WITH EXISTING AGGREGATION APPROACHES

Agg. types	Data need	Interpretability	Model simplification	Computation time	Accuracy	Challenges
Full [27]	Normal	Moderate	Low	Low	Low	Fails under LVRT; ignores wake effects and spatial diversity.
Semi [8], [28]	Normal	Good	Moderate	Moderate	Low	Sensitive to heuristic tuning; limited robustness.
Weighted [3], [12]	Normal	Good	Excellent	Moderate	Moderate	Sensitive to weighting selection; may lose dynamic diversity.
NN [29], [30]	High	Low	Moderate	Moderate	Moderate	Requires large datasets; black-box behaviour; slow training.
Physics-informed [13], [14]	Normal	Excellent	Excellent	High	Excellent	Boundary/initial conditions hard to define; convergence issues; high complexity.
Proposed	Low	Excellent	Excellent	Low	Excellent	Optimisation tuning needed; clustering depends on indicator selection.

where, $\lambda_i = 0.5$ is a conflict weight and $\epsilon = 10^{-10}$ is a small regularization term. The final descent direction is:

$$d = \frac{d_{\text{mod}} \odot \omega}{\|d_{\text{mod}} \odot \omega\|} \tag{29}$$

where $\odot$ represents element-wise multiplication.

7) Adaptive parameter update rule: The parameters are updated using the gradient descent rule with an adaptive learning rate:

$$\boldsymbol{\theta}^{(k+1)} = \mathcal{P}(\boldsymbol{\theta}^{(k)} - \alpha^{(k)}\mathbf{d}^{(k)}) \tag{30}$$

where:

- $\boldsymbol{\theta}^{(k)}$, $\alpha^{(k)}$, $\mathbf{d}^{(k)}$ represent parameter vector, learning rate, descent direction respectively at iteration k.
- $\mathcal{P}$ is the projection operator that enforces box constraints:

$$[\mathcal{P}(\boldsymbol{\theta})]_i = \max(\theta_i^L, \min(\theta_i^U, \theta_i)) \tag{31}$$

The learning rate is adapted based on the progress:

$$\alpha^{(k+1)} = \begin{cases} \max(\alpha^{(k)} \cdot 0.5, \alpha_{\min}) & \text{if } F_w(\boldsymbol{\theta}^{(k+1)}) > F_w(\boldsymbol{\theta}^{(k)}) \\ \min(\alpha^{(k)} \cdot 1.05, \alpha^{(0)}) & \text{if } F_w(\boldsymbol{\theta}^{(k+1)}) \leq F_w(\boldsymbol{\theta}^{(k)}) \end{cases} \tag{32}$$

When there's a significant increase in the objective function ($> 10\%$), the algorithm reverts completely to the previous parameter values .This is a safety mechanism to prevent large jumps in the wrong direction.

$$\boldsymbol{\theta}^{(k+1)} = \boldsymbol{\theta}^{(k)} \quad \text{if } F_w(\boldsymbol{\theta}^{(k+1)}) > 1.1 \cdot F_w(\boldsymbol{\theta}^{(k)}) \tag{33}$$

8) Cluster-based approach: The wind farm is partitioned into C clusters based on similarity of turbine characteristics:

$$\mathcal{W} = \bigcup_{c=1}^{C} \mathcal{W}_c \tag{34}$$

where, $\mathcal{W}_c$ is the set of turbines in cluster c.

For each cluster, a separate parameter identification problem is solved:

$$\boldsymbol{\theta}_c^* = \arg\min_{\boldsymbol{\theta}} F_w(\boldsymbol{\theta}; \mathcal{W}_c) \tag{35}$$

This refinement step tunes parameters within existing clusters to match the aggregated and detailed dynamic responses, without altering the established cluster structure. In addition, the parameters of collector lines, transformers, and other associated components are derived using aggregation techniques described in [8], [31].

Table I highlights the advantages and challenges of the proposed aggregation approach compared to existing methods, conventional full, semi-aggregated, weighted, neural network (NN), and physical informed models. The full and semi-aggregated models are computationally efficient but often lack sufficient accuracy and robustness under grid disturbances. While weighted and NN methods improve accuracy at the expense of sensitivity to weighting choices or reduced interpretability. Moreover, physics-informed approaches achieve high accuracy and interpretability by embedding physical knowledge, they typically require higher computational effort and face challenges related to boundary conditions and convergence. In contrast, the proposed method maintains an equally high level of accuracy and interpretability while significantly reducing data requirements and computational time through effective clustering and parameter reduction.

V. SIMULATION AND DISCUSSION

A. Simulation Model for Case Study

The wind farm model consists of 66×1.5 MW PMSGs ($WT_1 - WT_{66}$), whose layout and cable configuration are illustrated in Fig. 2. Each generator operates at a terminal voltage of 0.69 kV and is connected through a $35/0.69$ kV transformer ($T_1 - T_6$). The inter-turbine spacing is roughly 900–1300 meters inside the farm and around 600 meters at the periphery. Power from each string is collected via a 3 km medium voltage cable to the PCC, after which it is delivered to the grid through a 70 km, $35/220$ kV transformer. The detailed parameters of the PMSG and associated cables are provided in Appendix D.

B. WT Clustering Options

The WTs are clustered using the time series of clustering indicators under wind speed variations and fault disturbance. From Fig. 4, the optimal number of clusters is identified as $k = 3$ and $k = 4$ according to the AIC and BIC criterion, respectively. These values provide the lowest criterion value (AIC/BIC score) which is a trade-off between accuracy and simplicity (fewer clusters). To optimise performance, $k = 4$ is

obtained as the optimal value using ITA. This means whole WF can be represented by 4 clusters of aggregated WTs.

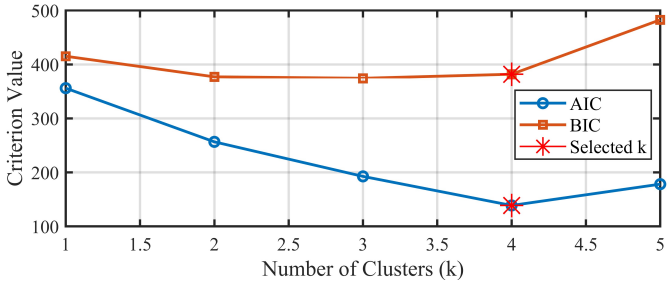

Fig. 4. Optimum number of cluster options.

The clustering outcomes obtained using the GMM algorithm are illustrated in Fig. 5, which compares the results with the classical time spot based clustering approach using $4s$ as the reference instant during wind speed disturbance. The proposed method produces a clearly distinct clustering structure. In contrast, time spot clustering differs (e.g., WT no: $4, 62, 63$ in cluster 4) because it captures turbine behaviour at a single time instant ($4s$ here) and assumes the operating characteristics remain unchanged over time, which leads to inconsistent grouping under dynamic conditions. To further validate the robustness of the proposed approach, a three-phase-to-ground fault is applied at the PCC from $8s$ to $8.2s$ in Fig. 2. The resulting clustering pattern under this fault disturbance is also shown in Fig. 5.

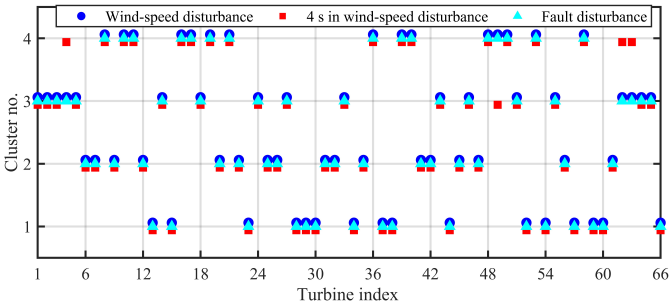

Fig. 5. Clustering results under wind speed disturbance, three phase fault and 4s time spot wind speed.

It is observed that the clustering options given for a fault disturbance and a wind speed disturbance are identical. This is because both wind disturbances and faults provoke dynamic responses in wind turbines like fluctuations in power output, shifts in terminal voltage. Although faults are more abrupt and severe, the nature of the system's response shares common patterns with those caused by wind variations. So, an accurate clustering options for WTs can be achieved by the proposed GMM based clustering method across both wind and fault scenarios.

TABLE II
CLUSTERING PERFORMANCE METRICS COMPARISON

Method	Silhouette	Intra-cluster variance
k-means	0.42	5.21
Fuzzy c-means	0.45	4.87
GMM–ITA (proposed)	**0.61**	**3.02**

In addition, Table II introduces a quantitative clustering benchmark comparing GMM–ITA, k-means, and fuzzy c-means, using silhouette score and intra-cluster variance as described in [32]. The results show that GMM–ITA achieves the highest silhouette score and lowest intra-cluster variance, indicating more coherent and better separated clusters and superior capture of wind turbine dynamic similarity.

C. Eigenvalue Sensitivity Analysis for System Parameters Selection

As outlined in Section III, Table III presents the eigenvalues and corresponding damping ratios from the small signal stability analysis.

TABLE III
EIGENVALUE SUMMARY WITH DAMPING RATIO AND FREQUENCY

Eigenvalue	Value	Damping (ζ)	Freq. (Hz)
$\lambda_{1,2}$	$-130.5051 + 498.5243j$	0.2532	79.34
λ_3	$-191.0960 + 0.0000j$	Non-oscillatory mode	
$\lambda_{4,5}$	$-61.1313 + 1.0502j$	0.9999	0.17
λ_6	$-36.0009 + 0.0000j$	Non-oscillatory mode	
λ_7	$-0.1362 + 0.0000j$	Non-oscillatory mode	
$\lambda_{8,9}$	$-0.0620 + 0.0002j$	1.0000	0.00
λ_{10}	$-0.0740 + 0.0000j$	Non-oscillatory mode	
λ_{11}	$-0.0746 + 0.0000j$	Non-oscillatory mode	
λ_{12}	$-0.3620 + 0.0000j$	Non-oscillatory mode	
λ_{13}	$-0.0277 + 0.0000j$	Non-oscillatory mode	
λ_{14}	$-0.0498 + 0.0000j$	Non-oscillatory mode	

The system is stable since all eigenvalues have real negative part. The eigenvalue analysis shows that eigenvalue $\lambda_{1,2}$ are oscillatory with a damping ratio of 0.2532, indicating decent damping; $\lambda_{4,5}$ exhibit high damping (0.9999) and extremely low frequency; and the remaining eigenvalues are non-oscillatory.

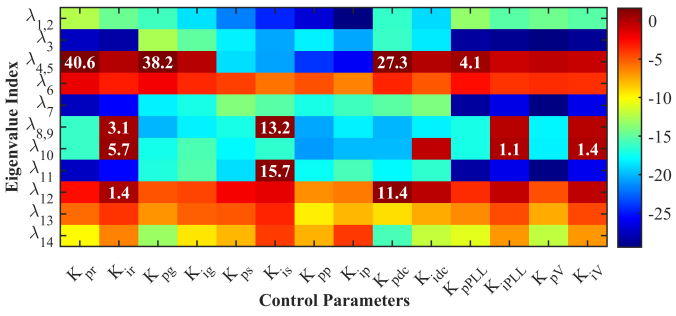

Fig. 6. Eigenvalue sensitivities to control parameters.

Fig. 6 presents a logarithmic scale heatmap illustrating the sensitivity of system eigenvalues to individual control parameters and highlighting values greater than 1. The results show that system dynamics are not uniformly affected by the control variables. Particularly, the dominant oscillatory mode ($\lambda_{4,5}$, λ_{11}) exhibit high sensitivity to (K_{pr}, K_{pg}, $K_{p_{dc}}$ and K_{is}) with peak values of 40.6, 38.2, and 27.3, 15.1 respectively, identifying them as the dominant control parameters. In contrast, K_{ir} displays a moderate but distributed influence across multiple modes ($\lambda_{8,9}$, λ_{10}, λ_{12}), indicating its role in overall system damping. The remaining control parameters

show consistently low sensitivity (e.g., K_{iPLL}, K_{iv}) and are therefore fixed at nominal values. By selecting only those parameters with high sensitivity, the optimisation process is directed toward variables that significantly influence system dynamics. This approach is further discussed in the following subsection.

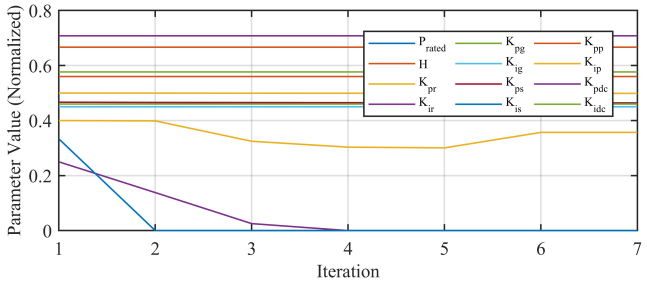

Fig. 7. Parameter evolution (normalised) for cluster 4.

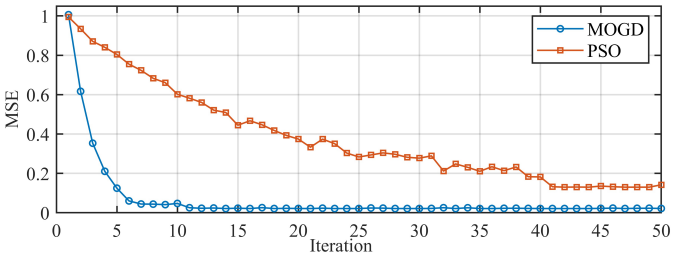

Fig. 8. Convergence curve of PSO and MOGD.

D. Optimum Parameters Identification by Proposed Method

The proposed multi-objective parameter identification algorithm successfully determines the key parameter value of four aggregated wind clusters under both wind speed variations and fault disturbances, as summarised in Table IV.

TABLE IV
OPTIMUM PARAMETERS IDENTIFIED FOR FOUR TURBINE CLUSTERS

Parameters	Cluster			
	1	2	3	4
P_{rated}	1.500000	1.500002	1.499998	1.499999
H	1.500001	0.900000	0.850000	1.000000
K_{pr}	0.849758	0.877602	0.859196	0.849993
K_{ir}	0.010000	0.010000	0.010000	0.010000
K_{pg}	7.730000	8.629999	9.230000	7.430001
K_{ig}	0.199000	0.198993	0.197885	0.200000
K_{ps}	0.934771	0.938193	1.179865	1.200000
K_{is}	0.003000	0.004000	0.005000	0.005000
K_{pp}	35.600000	42.700002	49.800000	44.340001
K_{ip}	0.007009	0.006899	0.006862	0.006902
K_{pdc}	13.540000	15.230000	17.210000	13.450001
K_{idc}	1.100004	2.130001	1.250000	1.250005

Fig. 7 shows that during the optimisation process, the K_{pr}, K_{pdc} and K_{is} parameters experience the most significant changes (cluster 4), suggesting they have a strong influence on the overall system behavior and were adjusted considerably to match the desired response. Similarly for Cluster 1: K_{pdc}, K_{is}; Cluster 2: K_{pdc}, K_{ir}; Cluster 3: K_{pr}, K_{pg}, K_{is}. This aligns with the eigenvalue-sensitivity analysis, which flagged these parameters as the most influential.

TABLE V
COMPARISON OF EVALUATION INDEXES OF DIFFERENT MODELS ACROSS UNKNOWN DISTURBANCES

Disturbance	Evaluation index	Multi-machine	Reduced order	Proposed	Detailed
Wind speed	MSE_P	1.01e–3	0.0049	2.14e–5	–
	MSE_Q	1.89e–3	2.35e–2	1.02e–6	–
FA	MSE_P	2.62e–2	0.008	2.93e–4	–
	MSE_Q	4.67e–4	0.0034	9.99e–7	–
FB	MSE_P	4.29e–4	1.44e–3	3.27e–7	–
	MSE_Q	2.12e–3	0.0089	4.38e–5	–
FC	MSE_P	5.64e–2	1.34e–2	4.32e–4	–
	MSE_Q	6.32e–3	0.0017	5.15e–5	–

To justify the choice, a convergence comparison between the proposed MOGD algorithm and PSO, in terms of MSE is presented in Fig. 8. Owing to the high computational cost of EMT level simulations, PSO is inefficient in this framework, whereas the proposed MOGD converges rapidly within 10 iterations. In contrast, PSO requires nearly 40 iterations to achieve even inferior MSE level.

E. Performance Evaluation of Proposed Model

To assess the robustness of the proposed WF aggregated model, we analysed its ability to represent dynamic responses under various unknown disturbance conditions. The specific characteristics of these disturbances are outlined below:

1) A gusty wind disturbance is introduced between $t = 8s$ and $t = 16s$. The wind speed profile rises from its initial value of 12 m/s to maximum at 21 m/s before returning to steady operation.

2) For the fault disturbance, the faults are: three-phase short circuit fault (FA), double line to ground fault (FB), single line to ground fault (FC), which occurs at the PCC at $8s$ and recovers at $8.2s$.

The performance of the proposed dynamic equivalent model is evaluated by calculating the mean square error (MSE) for the active and reactive power at the PCC, as MSE provides a robust measure for error evaluation. The formula used for this calculation is given by:

$$\text{MSE}_{P/Q} = \frac{1}{T}\sum_{t=1}^{T}\left(X(t) - \hat{X}(t)\right)^2 \tag{36}$$

Here, T is the total simulation time. $X(t)$ and $\hat{X}(t)$ are the values of active or reactive power from the proposed model and the detailed model, respectively, at any given time t.

Fig. 9 and Fig. 10 compare the dynamic responses of the multi-machine, reduced order, and the proposed aggregated model with the detailed model to demonstrate the effectiveness of the proposed method. The results indicate that the proposed model exhibits nearly identical transient responses to the detailed model, maintaining similar oscillation frequencies, damping characteristics, and steady-state convergence. The observed oscillations in figures arise from interactions between system inertia and dominant converter control parameters and are mitigated through the proposed MOGD-based tuning,

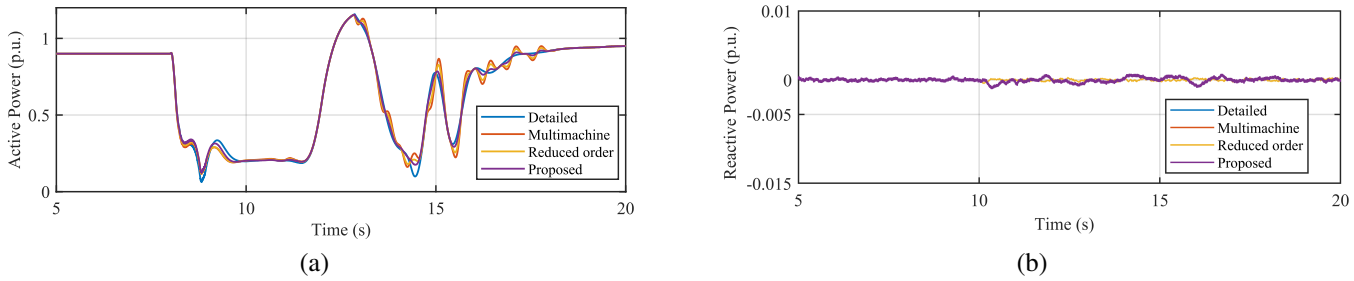

Fig. 9. Dynamic responses (a) active power under wind speed disturbance, (b) reactive power under wind speed disturbance.

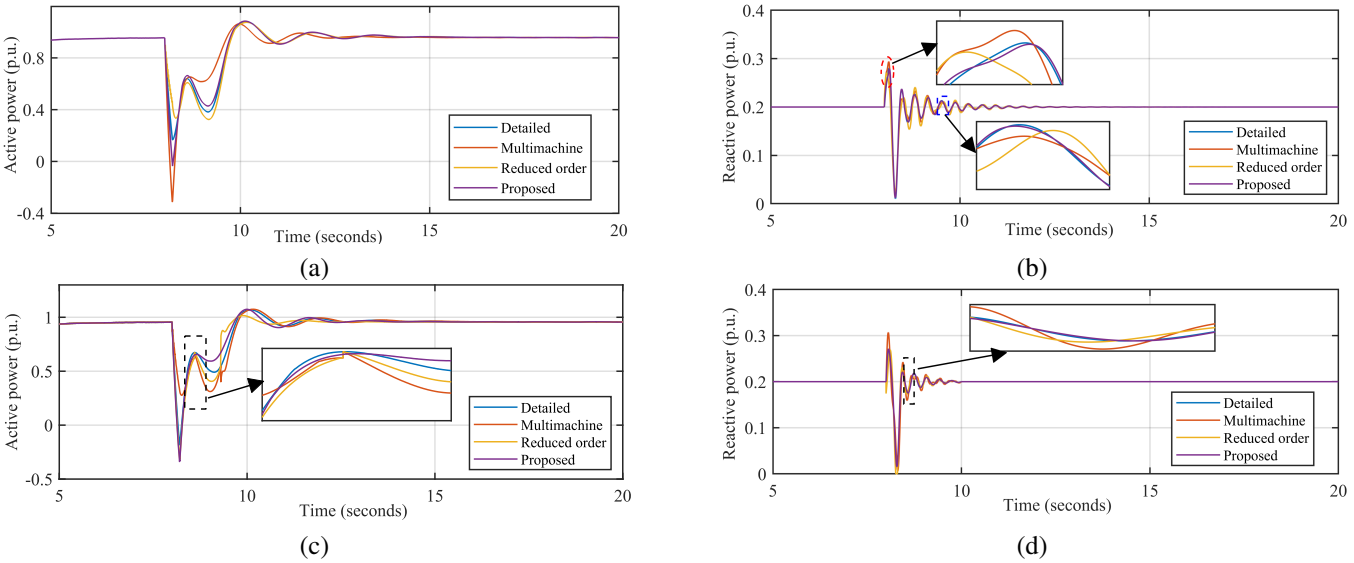

Fig. 10. Dynamic responses (a) active power under FA (b) reactive power under FA (c) active power under FB (d) reactive power under FB.

resulting in improved transient stability. Furthermore, the proposed method outperforms the multi-machine and reduced-order models by yielding the lowest MSE values for both active and reactive power (Table V), thereby accurately capturing wind turbine dynamics and nonlinear behaviour under wind and fault disturbances.

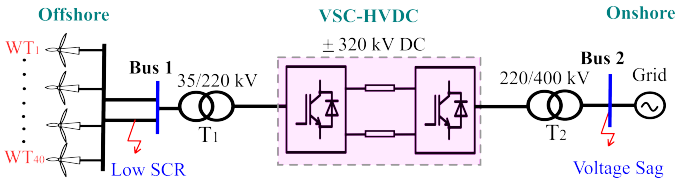

Fig. 11. PMSG based wind farm with HVDC transmission.

F. Applicability Test with HVDC system

To evaluate the model's applicability, the wind farm composed of 40 PMSGS is connected to Bus 1 through two offshore transmission lines, where its voltage is stepped up from 35 kV to 220 kV via transformer T_1. The aggregated power is then transferred through a ± 320 kV VSC-HVDC link and stepped up the voltage to connect with the onshore side. The complete system layout is illustrated in Fig. 11. The detailed HVDC modelling methodology is based on [33] and corresponding parameters are given in Appendix D. To assess the effectiveness of the proposed aggregated model, two representative operating conditions are investigated: a severe disturbance by a voltage sag at bus 2, and a weakly damped condition produced by disconnecting the line at bus 1.

1) Voltage Sag test: Under normal operation, a three-phase voltage dip to 0.3 p.u. is imposed at bus 2 at $t = 6.4s$ for a duration of $0.1s$, and the resulting active and reactive power responses from both the detailed wind farm and the aggregated model are compared with those obtained using the reduced-order method, as shown in Fig. 12. The aggregation process reduces the model size from 560 (14 states per turbine) states to only 34, yielding a substantial improvement in computational efficiency. The proposed model significantly reduces simulation time; a 4-second simulation, which took $1013.2s$ with the detailed model, is completed in only $24.13s$. Crucially, this speed increase does not sacrifice accuracy, as demonstrated by low MSE values of 0.0025 (active power) and 0.0019 (reactive power). The proposed method successfully retains the dominant multi-time-scale dynamics of the wind farm as verified in Fig. 12.

2) Weak grid test: This section examines the performance of the proposed aggregated model under weak grid conditions through small-signal stability analysis. The system short circuit ratio (SCR) is intentionally reduced by disconnecting one transmission line at the wind farm PCC, after which the corresponding active power response is presented in Fig. 13(a) and shows clear oscillatory characteristics. Fourier analysis

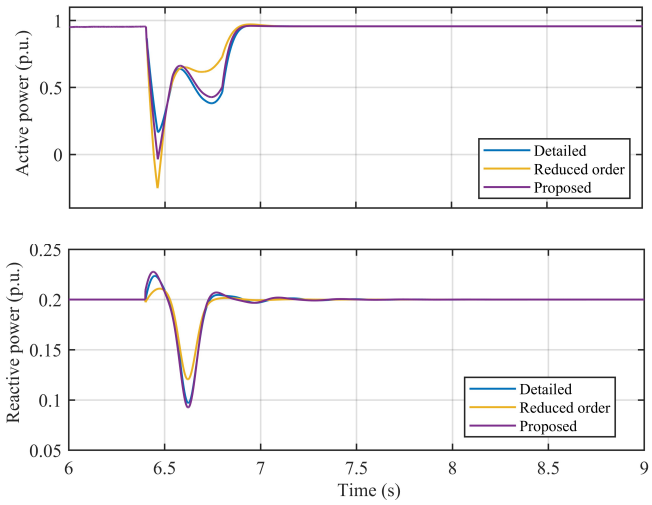

Fig. 12. Comparison in time domain under voltage sag.

of the signal between $4.3s$ and $4.7s$ identifies two major spectral components at 68.31 Hz and 154.95 Hz as shown in 13(b). To further analyse these dynamics, the aggregated wind farm and the HVDC system are linearised to $4.8s$ to derive the state space model, from which the system poles are obtained and displayed in Fig. 14. The results indicate that the lower frequency mode of 67.1 Hz is well damped (real part -20), while the higher frequency mode of 155.7 Hz is unstable (real part 8), consistent with observations from the time and frequency domain responses. Moreover, the reduced order model successfully reproduces the dominant oscillatory behavior observed in the full order system, confirming that the proposed aggregation approach accurately represents the wind farm's small signal dynamics.

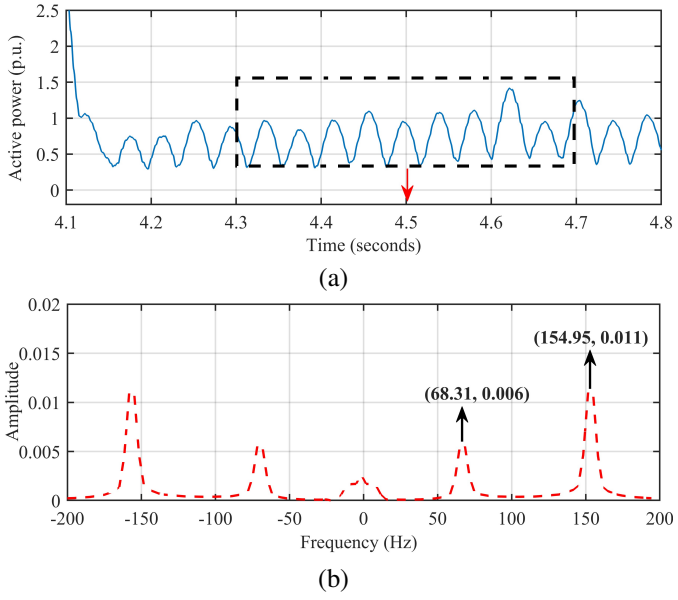

Fig. 13. (a) Wind farm active power (b) corresponding Fourier spectrum.

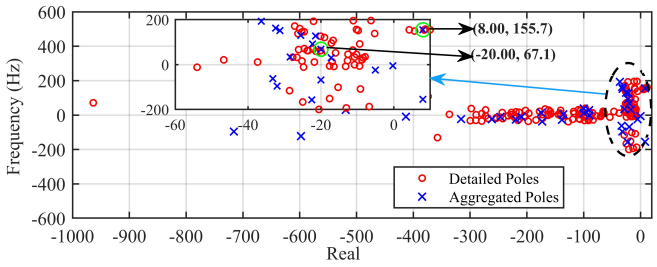

Fig. 14. Comparison of pole distributions for aggregated and detailed wind farm models.

G. Grid Compliance Assessment of Proposed Aggregated Model

This subsection compares performance of the detailed and aggregated model under GCO141 modelling requirement by UK ESO. GCO141 mandates that the enhanced model must demonstrate high fidelity with pre-event (3% error) and post-event (3% error) phases, while also capturing transient behavior within a ±10% envelope and exhibiting similar trends.

1) Voltage control validation: As per UK grid code ECP.A.3.7.4 [34], the model must simulate a ±2% voltage reference step at the controller responsible for voltage control at the point of connection. This test must demonstrate compliance with the dynamic response requirements of ECC.A.7.2.3 [19].

Upon experiencing a 2% voltage rise at $0.5s$ as shown in Fig. 15, the system increases its reactive power absorption by 0.004 p.u. Conversely, when subjected to a 2% voltage reduction, the WF decreases its reactive power absorption by 0.003 p.u. The aggregated model exhibits a steady-state voltage deviation of only 0.2%, well within the ±3% limit. Reactive power initiation occurs within 100 ms, providing a substantial margin below the 200 ms requirement.

2) Fault Ride Through Validation: To demonstrate compliance with the UK grid code fault ride-through (FRT) requirements, the generating unit must withstand a range of fault events without disconnection from the system. As part of the GCO141 testing process, specific fault ride-through scenarios are simulated, as defined by the FRT voltage-against-time curve in grid code ECC.6.3.15 [19], [34]. The tests are follow:

- A three phase balanced fault, double-phase-to-ground fault and single-phase-to-ground fault at the point of connection lasting 140 ms.
- A balanced 80% voltage dip lasting $2.5s$.

Once the fault is cleared, the voltage at the point of connection should return to near pre-fault levels within a few hundred milliseconds. In addition, the active power output of the generator must recover to at least 90% of its pre-fault value within 500 ms after the voltage restoration. All these cases are verified in Fig. 16, applying faults at $0.5s$ and clear at $0.64s$. This demonstrates the aggregated model achieves a recovery of 94% within 450 ms, satisfying the requirement by providing a 4% power margin and 50 ms timing margin against GCO141 threshold criteria.

3) RoCoF Requirement: According to the UK grid code ECC.6.3.7/DRSC 5.1, generating units must be capable of

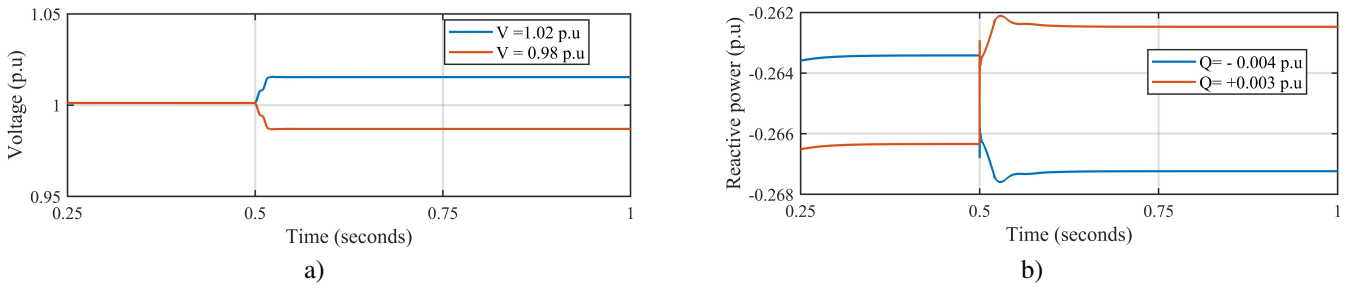

Fig. 15. Dynamic responses (a) active power under wind speed disturbance, (b) reactive power under wind speed disturbance.

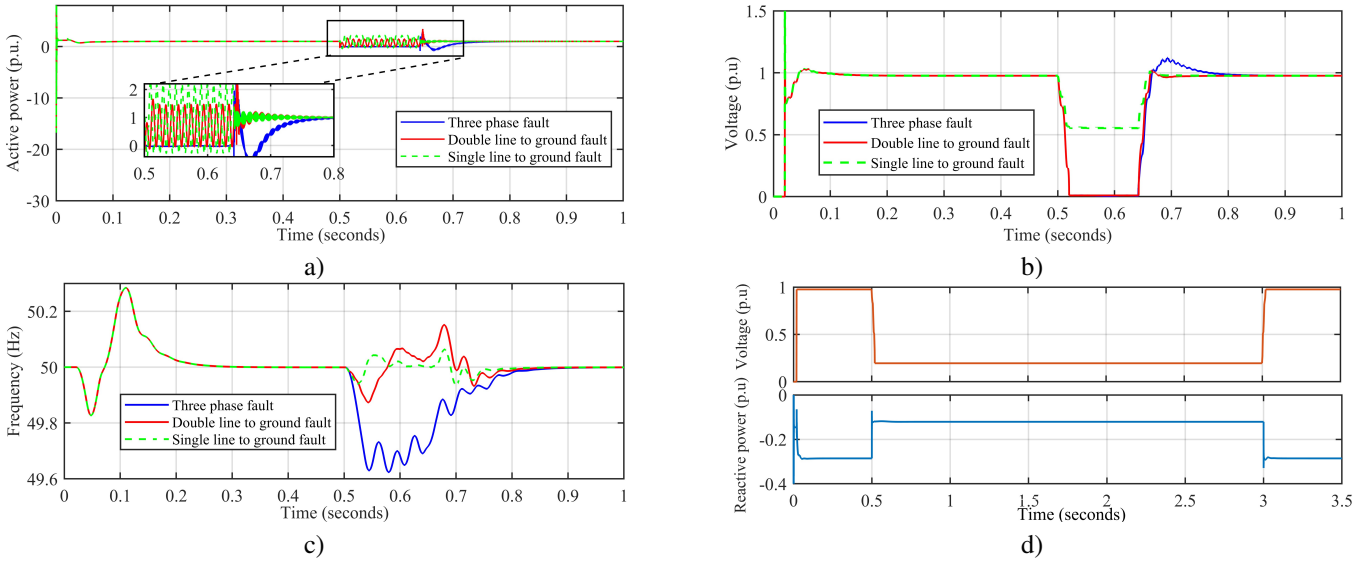

Fig. 16. Dynamic responses of the aggregated model according to GCO141 for FRT requirement at PCC (a) active power (b) PCC voltage (c) frequency (d) extended voltage dip test.

withstanding RoCoF values up to at least ±1 Hz/s measured over a 500 ms rolling average window at the connection point, without tripping. For each fault type shown in the Fig. 16(c), RoCoF using the standard 500 ms measurement window is calculated (0.5-1 s). The RoCoF are -0.74 Hz/s,-0.26 Hz/s and -0.1 Hz/s for three phase fault, double line to ground fault and single line to ground fault respectively, which lies within the ±1 Hz/s grid code limits.

4) Impact of modelling fidelity on Critical Clearing Time (CCT): The calculated CCT is a critical stability index for system operators. When the WF is represented using detailed models, the CCT is determined to be 260 ms, whereas it deteriorates to 230 ms under aggregated modelling, as shown in Fig. 17. In the aggregated case, inaccuracies in the simulated power modulation behaviour can significantly affect the system's CCT. Moreover, if the CCT exceeds a certain threshold, the aggregated system loses stability because the grid residual voltage fails to recover following fault clearing, while the detailed system is able to preserve stability.

A three-phase fault is first applied at $0.3s$ and cleared at $0.4s$, during which both the detailed and aggregated model remain stable. A second fault is applied at $0.7s$, with clearance at $0.93s$ for the aggregated model and $0.96s$ for the detailed model. After this event, the detailed model maintains stability, whereas the aggregated model becomes unstable as shown in Fig. 17(a). This is caused by the residual voltage of WF behaves abnormally after fault clearance, followed by a sharp divergence, clearly indicating occurrence of a instability. Simultaneously, WFs lose controllability on electrical power which shown in Fig. 17(c), 17(d). The underestimation of CCT primarily results from the aggregated model's inability to fully capture turbine level nonuniformity during transient events. This leads to inaccurate power modulation under fault conditions, typically overestimating the remaining active power that reduces rotor acceleration and accelerates the power angle swing. In addition, these power modulation errors combined with the controlled power source nature of wind turbine generator, trigger singularity induced instability. The singularity occurs when the system sensitivity matrix becomes singular, causing voltage divergence [21].

The discrepancy between detailed and aggregated model during post fault recovery highlights the need for accurate modelling when assessing UK grid code compliance. Simplified models can misrepresent dynamic stability, potentially masking violations of CC.6.1.7, which requires voltage to stay within ±10% of nominal at transmission levels.

H. Computational Time Enhancement

The computational efficiency of the proposed aggregated model, in comparison to the detailed model, was assessed

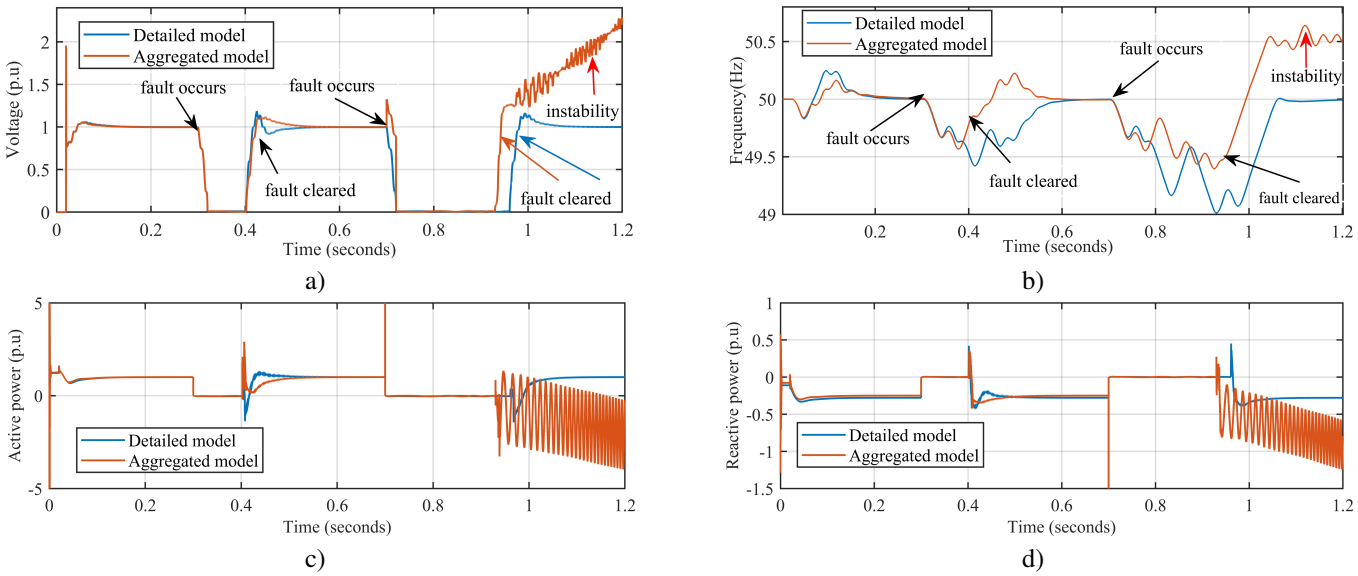

Fig. 17. Instability signified by voltage divergence (a) grid residual voltage (b) frequency at PCC (c) active power and (d) reactive power

based on their respective simulation times. The evaluation process consists of two main stages: first, identifying optimal cluster configurations using GMM, and second, performing parameter identification through an optimisation algorithm. Both Detailed EMT and aggregated simulations were conducted in MATLAB/Simulink R2023b. The stiff solver ODE8 (Dormand-Prince) was adopted with a fixed time step of 20 µs for the detailed model and an adaptive configuration with the same maximum step size for the aggregated model. All simulations were carried out on a Dell Latitude 5440 equipped with 16 GB of RAM and a 13th Gen Intel® Core™ i7-1355U processor running at 1.7 GHz on a 64-bit Windows 11 operating system. For consistency, all models were compared using the same number of wind turbines and identical device configurations. By reducing the parameter space to only the dominant parameters, convergence is achieved within 7–10 iterations, with total optimisation times ranging from $0.004s$ to $0.0021s$, as shown in Table VI. The proposed model achieves a speed-up of over 2100 times faster than the detailed model and approximately twice as fast as the fastest reduced-order model available in the literature to date, as reported in Table VII.

TABLE VI
COMPUTATIONAL TIME BREAKDOWN FOR PARAMETER IDENTIFICATION

Cluster	Iterations	Total Time (seconds)
Cluster 1	8	0.016
Cluster 2	10	0.006
Cluster 3	10	0.004
Cluster 4	7	0.0021

TABLE VII
COMPARISON OF COMPUTATIONAL TIME FOR 1 S SOLVING WITH DIFFERENT MODELS

Aggregation types	Computational time (seconds)
Proposed model	0.1681
Detailed model	354
Multi-machine model [2]	12.57
Reduced order model [35]	0.306

VI. CONCLUSION

This paper presents a novel dynamic aggregation methodology for PMSG-based offshore wind farms, effectively balancing model accuracy and computational efficiency. By employing GMM based clustering with ITA, the approach successfully identifies an optimal set of representative wind turbine clusters reducing the total from 11 in the detailed EMT model to just 4. The integration of structured eigenvalue sensitivity analysis enhances the understanding of critical control parameters influencing system dynamics. Furthermore, a refined multi-objective gradient descent optimisation technique ensures robust parameter tuning across varying wind and fault scenarios.

Validation against UK GCO141 modelling standards confirms the aggregated model's ability to closely replicate both dynamic and steady-state behavior of the full EMT model, while achieving a remarkable 2100 fold reduction in computational burden. In the HVDC-connected case, the proposed model also preserves key time-domain transients and dominant frequency-domain modes under large and small disturbance, proving its applicability beyond AC network studies. However, aggregated models may incorrectly estimate the CCT due to instability from residual voltage recovery after fault clearance. This discrepancy underscores the need for careful interpretation of aggregation results in stability assessments and grid code compliance studies.

In addition, the proposed methodology is fully compatible with long term historical datasets and can be extended to incorporate extensive Supervisory Control and Data Acquisition (SCADA) or PMU records, when such data become available. Future work will focus on extending the methodology to capture multi-string behaviour and cable interconnection diversity, thereby refining fault-induced dynamics to improve the CCT prediction accuracy of aggregated models.

APPENDIX

A. Nomenclature

ω_r	Rotor speed
β	Pitch angle
i_{dr}, i_{qr}	Rotor-side d- and q-axis currents
i_{dg}, i_{qg}	Grid-side d- and q-axis currents
V_{dc}	DC-link voltage
$i_{\text{int},dr}$, $i_{\text{int},qr}$	Integral states of rotor side current controllers
$i_{\text{int},dg}$, $i_{\text{in,t}qg}$	Integral states of grid side current controllers
$i_{\text{int},V_{dc}}$	Integral state of DC-link voltage controller
i_{int,ω_r}	Integral state of rotor speed controller
$i_{\text{int},\theta}$	Integral state of pitch controller
$i_{dr,\text{ref}}$, $i_{qr,\text{ref}}$	References for rotor-side d- and q-axis currents
$i_{dg,\text{ref}}$, $i_{qg,\text{ref}}$	References for grid-side d- and q-axis currents
$V_{dc,\text{ref}}$	Reference DC-link voltage
β_{ref}	Reference pitch angle
$\omega_{r,\text{ref}}$	Reference rotor speed
K_{pr}, K_{ir}	PI gains of rotor side current controller
K_{pg}, K_{ig}	PI gains of grid side current controller
K_{ps}, K_{is}	PI gains of speed controller
K_{pp}, K_{ip}	PI gains of pitch controller
K_{pdc}, K_{idc}	PI gains of DC-link voltage controller
K_{pPLL}, K_{iPLL}	PI gains of PLL
K_{pv}, K_{iv}	PI gains of reactive power controller
P_{rated}	Rated power
H	Inertia constant

B. PMSG based Single Wind Turbine State Space Modelling

1) **Model of drivetrain aerodynamics:**

$$\frac{d\omega_r}{dt} = \frac{1}{J}\left(T_{mech} - T_{em}\right) \tag{37}$$

2) **Pitch controller dynamics:**

$$\frac{d\beta}{dt} = K_{pp}\left(\omega_{ref} - \omega_r\right) + K_{ip}\int\left(\omega_{ref} - \omega_r\right)dt \tag{38}$$

$$\frac{d}{dt}\int\left(\omega_{ref} - \omega_r\right) = \omega_{ref} - \omega_r \tag{39}$$

3) **Rotor side converter dynamics:**

$$\frac{di_{dr}}{dt} = \frac{1}{L_d}\Big[K_{p,dr}(i_{dr,ref} - i_{dr}) + K_{i,dr}\int(i_{dr,ref} - i_{dr})dt - R_r i_{dr} + \omega_r L_q i_{qr}\Big] \tag{40}$$

$$\frac{di_{qr}}{dt} = \frac{1}{L_q}\Big[K_{p,qr}(i_{qr,ref} - i_{qr}) + K_{i,qr}\int(i_{qr,ref} - i_{qr})dt + R_r i_{qr} + \omega_r(L_d i_{dr} + \lambda_m)\Big] \tag{41}$$

$$\frac{d}{dt}\int(i_{dr,ref} - i_{dr}) = i_{dr,ref} - i_{dr} \tag{42}$$

$$\frac{d}{dt}\int(i_{qr,ref} - i_{qr}) = i_{qr,ref} - i_{qr} \tag{43}$$

4) **Grid side converter dynamics:**

$$\frac{di_{dg}}{dt} = \frac{1}{L_g}\Big[K_{p,dg}(i_{dg,ref} - i_{dg}) + K_{i,dg}\int(i_{dg,ref} - i_{dg})dt + R_g i_{dg} - \omega_g L_g i_{qg} + V_{gd}\Big] \tag{44}$$

$$\frac{di_{qg}}{dt} = \frac{1}{L_g}\Big[K_{p,qg}(i_{qg,ref} - i_{qg}) + K_{i,qg}\int(i_{qg,ref} - i_{qg})dt + R_g i_{qg} + \omega_g L_g i_{dg} + V_{gq}\Big] \tag{45}$$

$$\frac{d}{dt}\int\left(i_{dg,ref} - i_{dg}\right)dt = i_{dg,ref} - i_{dg} \tag{46}$$

$$\frac{d}{dt}\int\left(i_{qg,ref} - i_{qg}\right)dt = i_{qg,ref} - i_{qg} \tag{47}$$

5) **DC-link dynamics:**

$$\frac{dV_{dc}}{dt} = \frac{i_{dr} - i_{dg}}{C_{dc}} \tag{48}$$

$$\frac{d}{dt}\int\left(V_{dc,ref} - V_{dc}\right)dt = V_{dc,ref} - V_{dc} \tag{49}$$

This all defining the detailed physics of a single aggregated turbine cluster.

C. Aggregated Wind Farm State-Space Model

For each cluster $k = 1, \ldots, K$ (one PMSG-based equivalent per cluster), define:

- $X^{(k)} \in \mathbb{R}^{n_k}$: state vector (e.g., ω_r, β, i_{dr}, i_{qr}, i_{dg}, i_{qg}, V_{dc} and controller integrators).
- $U^{(k)} \in \mathbb{R}^{m_k}$: input vector ($i_{dr,\text{ref}}$, $i_{qr,\text{ref}}$, $i_{dg,\text{ref}}$, $i_{qg,\text{ref}}$, $V_{dc,\text{ref}}$, β_{ref}, $\omega_{r,\text{ref}}$).
- $V^{(k)}$, $I^{(k)}$: terminal voltage and current of the cluster at its collector node.

Step 1: Per-cluster model

$$\dot{X}^{(k)} = A^{(k)}X^{(k)} + B^{(k)}U^{(k)} + E^{(k)}V^{(k)} \tag{50}$$

$$I^{(k)} = C^{(k)}X^{(k)} + D^{(k)}U^{(k)} + F^{(k)}V^{(k)} \tag{51}$$

Here, system matrices for the cluster are: $A^{(k)}$(state), $B^{(k)}$(input), $E^{(k)}$(voltage coupling), $C^{(k)}$(state to current), $D^{(k)}$(input to current), $F^{(k)}$(voltage to current).

Step 2 :Stack all clusters

$$X = \left[X^{(1)}; \ldots; X^{(K)}\right], \quad U = \left[U^{(1)}; \ldots; U^{(K)}\right],$$
$$V = \left[V^{(1)}; \ldots; V^{(K)}\right], \quad I = \left[I^{(1)}; \ldots; I^{(K)}\right]$$

Using (50)-(51), the farm-level plant is:

$$\dot{X} = AX + BU + EV \tag{52}$$

$$I = CX + DU + FV \tag{53}$$

Step 3: Collector-network coupling

Let Y_{col} be the nodal admittance matrix of the collector system (strings, cables, transformers, PCC model):

$$I = Y_{\text{col}}V \tag{54}$$

Step 4: Differential–algebraic form
Combining (53) with (54):

$$(Y_{\text{col}} - F)V = CX + DU \tag{55}$$

Together with (53), the farm is a differential-algebraic system

$$\dot{X} = AX + BU + EV \tag{56}$$

$$0 = (Y_{\text{col}} - F)V - (CX + DU) \tag{57}$$

Step 5: Eliminate algebraic voltages
If $(Y_{\text{col}} - F)$ is nonsingular,

$$V = (Y_{\text{col}} - F)^{-1}(CX + DU) \tag{58}$$

Substituting (58) into (56) yields a pure ODE:

$$\dot{X} = A_{\text{agg}}X + B_{\text{agg}}U \tag{59}$$

with aggregated matrices

$$A_{\text{agg}} = A - E(Y_{\text{col}} - F)^{-1}C \tag{60}$$

$$B_{\text{agg}} = B - E(Y_{\text{col}} - F)^{-1}D \tag{61}$$

This (A_{agg}, B_{agg}) is the final aggregated wind farm state-space.

D. Parameters of the model

TABLE VIII
SYSTEM PARAMETERS FOR CASE STUDY [5], [35]

System	Parameter	Value
PMSG	Rated power P_{rated} (MW)	1.5
	Stator resistance R_s (p.u.)	0.0272
	Stator reactance L_s(p.u.)	0.5131
	Inertia constant (s)	1.4393
	DC bus voltage (V)	1150
	DC capacitor C_{bus} (F)	0.01
	Filter resistance R_g (Ω)	0.03
	Filter inductance L_g (H)	0.3
Cable parameters	WT cable resistance (Ω/km)	0.124
	WT cable reactance (mH/km)	0.39
	MV cable resistance (Ω/km)	0.36
	MV cable reactance (mH/km)	0.32
	Submarine cable resistance (Ω/km)	0.34
	Submarine cable reactance (mH/km)	0.17
VSC–HVDC	Rated AC voltage (kV)	400
	HVDC voltage (kV)	±320
	DC link capacitor (μF)	500
	Filter inductance (H)	0.0032
	Filter resistance (Ω)	0.075
	DC line resistance (Ω)	0.29
	DC line inductance (H)	0.0079

REFERENCES

[1] V. Jalili-Marandi, L.-F. Pak, and V. Dinavahi, "Real-time simulation of grid-connected wind farms using physical aggregation," *IEEE Transactions on industrial electronics*, vol. 57, no. 9, pp. 3010–3021, 2009.

[2] A. P. Gupta, A. Mitra, A. Mohapatra, and S. N. Singh, "A multi-machine equivalent model of a wind farm considering lvrt characteristic and wake effect," *IEEE Transactions on Sustainable Energy*, vol. 13, no. 3, pp. 1396–1407, 2022.

[3] Y. Zhou, L. Zhao, I. B. Matsuo, and W.-J. Lee, "A dynamic weighted aggregation equivalent modeling approach for the dfig wind farm considering the weibull distribution for fault analysis," *IEEE Transactions on Industry Applications*, vol. 55, no. 6, pp. 5514–5523, 2019.

[4] J. Martínez-Turégano, S. Añó-Villalba, S. Bernal-Perez, and R. Blasco-Gimenez, "Aggregation of type-4 large wind farms based on admittance model order reduction," *Energies*, vol. 12, no. 9, p. 1730, 2019.

[5] J. Zou, C. Peng, H. Xu, and Y. Yan, "A fuzzy clustering algorithm-based dynamic equivalent modeling method for wind farm with dfig," *IEEE transactions on energy conversion*, vol. 30, no. 4, pp. 1329–1337, 2015.

[6] C. Guo, F. Gan, D. Du, Y. Guo, and H. Cheng, "Applicability evaluation of wind farm impedance models using different aggregation methods for high frequency oscillation analysis," *IEEE Transactions on Power Delivery*, vol. 39, no. 4, pp. 2231–2241, 2024.

[7] P. Wang, Z. Zhang, Q. Huang, N. Wang, X. Zhang, and W.-J. Lee, "Improved wind farm aggregated modeling method for large-scale power system stability studies," *IEEE Transactions on Power Systems*, vol. 33, no. 6, pp. 6332–6342, 2018.

[8] Y. Zhou, L. Zhao, and W.-J. Lee, "Robustness analysis of dynamic equivalent model of dfig wind farm for stability study," *IEEE Transactions on Industry Applications*, vol. 54, no. 6, pp. 5682–5690, 2018.

[9] Y. Wang, C. Lu, L. Zhu, G. Zhang, X. Li, and Y. Chen, "Comprehensive modeling and parameter identification of wind farms based on wide-area measurement systems," *Journal of Modern Power Systems and Clean Energy*, vol. 4, no. 3, pp. 383–393, 2016.

[10] D.-E. Kim and M. A. El-Sharkawi, "Dynamic equivalent model of wind power plant using parameter identification," *IEEE Transactions on Energy Conversion*, vol. 31, no. 1, pp. 37–45, 2015.

[11] J. Yuqing, J. Ping, and P. Xueping, "Analysis on controller aggregation method for equivalent modeling of dfig-based wind farm," *Automation of Electric Power Systems*, vol. 38, no. 3, pp. 19–24, 2014.

[12] N. Shabanikia, A. A. Nia, A. Tabesh, and S. A. Khajehoddin, "Weighted dynamic aggregation modeling of induction machine-based wind farms," *IEEE Transactions on Sustainable Energy*, vol. 12, no. 3, pp. 1604–1614, Apr. 2021.

[13] H. Wang, Z. Yang, W. Kang, P. Sun, G. Konstantinou, and Z. Chen, "Physics-informed learning based wind farm two-machine aggregation model for large-scale power system stability studies," *IEEE Transactions on Power Systems*, 2024.

[14] X. Shi, D. Guo, W. Wang, Y. Cao, M. Shi, Y. Li, and L. Zhou, "Physical-informed detailed aggregation of wind farm based on symbolic regression: Structure, solution and generalizability," *IEEE Transactions on Sustainable Energy*, 2025.

[15] J. Stiasny, G. S. Misyris, and S. Chatzivasileiadis, "Physics-informed neural networks for non-linear system identification for power system dynamics," in *2021 IEEE Madrid PowerTech*. IEEE, 2021, pp. 1–6.

[16] N. Cassamo and J.-W. van Wingerden, "Model predictive control for wake redirection in wind farms: a koopman dynamic mode decomposition approach," in *2021 American Control Conference (ACC)*. IEEE, 2021, pp. 1776–1782.

[17] G. Chen, H. Zhang, H. Hui, and Y. Song, "Deep-quantile-regression-based surrogate model for joint chance-constrained optimal power flow with renewable generation," *IEEE Transactions on Sustainable Energy*, vol. 14, no. 1, pp. 657–672, 2022.

[18] H. W. J. Chen, W. DU, "A data-driven method for oscillation stability assessment of grid-connected wind farm based on dynamic parameters equivalent," *Proceedings of the CSEE*, 2022, 42(19): 6958-6973.

[19] National Grid Electricity System Operator, "GC0141: Compliance Processes and Modelling Amendments Following 9th August Power Disruption," Available at: neso.energy/gc0141, 2022, accessed: 2025-08-22.

[20] J. Ekanayake and N. Jenkins, "Comparison of the response of doubly fed and fixed-speed induction generator wind turbines to changes in network frequency," *IEEE Transactions on Energy conversion*, vol. 19, no. 4, pp. 800–802, 2004.

[21] J.-Y. Ruan, Z.-X. Lu, Y. Qiao, and Y. Min, "Analysis on applicability problems of the aggregation-based representation of wind farms considering dfigs' lvrt behaviors," *IEEE Transactions on Power Systems*, vol. 31, no. 6, pp. 4953–4965, 2016.

[22] H. Wan, H. Wang, B. Scotney, and J. Liu, "A novel gaussian mixture model for classification," in *2019 IEEE International Conference on Systems, Man and Cybernetics (SMC)*. IEEE, 2019, pp. 3298–3303.

[23] L. Bottou, "Large-scale machine learning with stochastic gradient descent," in *Proceedings of COMPSTAT'2010: 19th International Conference on Computational StatisticsParis France, August 22-27, 2010 Keynote, Invited and Contributed Papers*. Springer, 2010, pp. 177–186.

[24] K. P. Burnham, D. R. Anderson, K. P. Burnham, and D. R. Anderson, *Practical use of the information-theoretic approach*. Springer, 1998.

[25] Y. Tang, P. Ju, H. He, C. Qin, and F. Wu, "Optimized control of dfig-based wind generation using sensitivity analysis and particle swarm

optimization," *IEEE Transactions on Smart Grid*, vol. 4, no. 1, pp. 509–520, 2013.

[26] H. Xie, P. Ju, J. Luo, Y. Ning, H. Zhu, and X. Wang, "Identifiability analysis of load parameters based on sensitivity calculation," *Automation of Electric Power Systems*, vol. 33, no. 7, pp. 17–21, 2009.

[27] L. P. Kunjumuhammed, B. C. Pal, C. Oates, and K. J. Dyke, "The adequacy of the present practice in dynamic aggregated modeling of wind farm systems," *IEEE Transactions on Sustainable Energy*, vol. 8, no. 1, pp. 23–32, 2016.

[28] W. Li, I. Kaffashan, A. M. Gole, and Y. Zhang, "Structure preserving aggregation method for doubly-fed induction generators in wind power conversion," *IEEE Transactions on Energy Conversion*, vol. 37, no. 2, pp. 935–946, 2021.

[29] T. Xiao, Y. Chen, S. Huang, T. He, and H. Guan, "Feasibility study of neural ode and dae modules for power system dynamic component modeling," *IEEE Transactions on Power Systems*, vol. 38, no. 3, pp. 2666–2678, 2022.

[30] K. Chen, J. Lin, Y. Qiu, F. Liu, and Y. Song, "Model predictive control for wind farm power tracking with deep learning-based reduced order modeling," *IEEE Transactions on Industrial Informatics*, vol. 18, no. 11, pp. 7484–7493, 2022.

[31] L. Li, T. Wang, and X. Wang, "Dynamic equivalent modeling of wind farm with ddpmsg wind turbine generators," in *2014 International Conference on Power System Technology*. IEEE, 2014, pp. 2908–2914.

[32] A. Punhani, N. Faujdar, K. K. Mishra, and M. Subramanian, "Binning-based silhouette approach to find the optimal cluster using k-means," *IEEE Access*, vol. 10, pp. 115 025–115 032, 2022.

[33] S. K. Chaudhary, R. Teodorescu, P. Rodriguez, P. Kjær, and P. Christensen, "Modelling and simulation of vsc-hvdc connection for wind power plants," in *Proceeding of the 5th Nordic Wind Power Conference: Power System Integration and Electrical Systems of Wind Turbines and Wind Farms*, 2009.

[34] National Grid Electricity System Operator, "The Complete Grid Code," https://dcm.nationalenergyso.com/, 2025, accessed: 2025-05-22.

[35] M. G. Taul, X. Wang, P. Davari, and F. Blaabjerg, "Reduced-order and aggregated modeling of large-signal synchronization stability for multiconverter systems," *IEEE Journal of Emerging and Selected Topics in Power Electronics*, vol. 9, no. 3, pp. 3150–3165, 2020.